



# Dipeptidyl peptidase 11



## A Target Enabling Package (TEP)

Gene ID / UniProt ID / EC	<a href="#">PGN_RS02895</a> , <a href="#">B2RID1</a> / <a href="#">EC 3.4.14</a>
Target Nominator	Centre for Medicines Discovery (University of Oxford, UK)
Authors	Catherine Tham <sup>1</sup> , Jesse Coker <sup>1</sup> , William Foster <sup>1</sup> , Tobias Krojer <sup>1</sup> , Lizbe Koekomer <sup>1</sup> , Yuko Ohara-Nemoto <sup>2</sup> , Takayuki K. Nemoto <sup>2</sup> , Wyatt W. Yue <sup>1</sup> , Frank von Delft <sup>1</sup> , Gustavo Arruda Bezerra <sup>1</sup>
Target PI	Gustavo Arruda Bezerra (CMD Oxford)
Therapeutic Area(s)	Infectious diseases
Disease Relevance	DPP11 is a protease central to the energy metabolism of <i>Porphyromonas gingivalis</i> , the main causative agent of Periodontitis.
Date Approved by TEP Evaluation Group	June 2 <sup>nd</sup> 2021
Document version	1.0
Document version date	Feb 2022
Citation	<a href="https://doi.org/10.5281/zenodo.6281991">https://doi.org/10.5281/zenodo.6281991</a>
Affiliations	<sup>1</sup> Centre for Medicines Discovery, Nuffield Department of Medicine, University of Oxford. <sup>2</sup> Department of Oral Molecular Biology, Nagasaki University.

### USEFUL LINKS



(Please note that the inclusion of links to external sites should not be taken as an endorsement of that site by the CMD in any way)

### SUMMARY OF PROJECT

*Porphyromonas gingivalis* (*P. gingivalis*) is the main causative agent of Periodontitis, the most widespread inflammatory condition world-wide. Recently this organism has been implicated in

several systemic conditions, such as Alzheimer's disease and type 2 diabetes. *P. gingivalis* does not ferment carbohydrates, instead it uses proteases to generate energy and carbon source. Dipeptidyl peptidase 11 plays a central role in the energy metabolism of this bacterium and has been proposed as an attractive drug target. This TEP provide early tools to develop inhibitors of PgDPP11, including purification protocols of recombinant proteins, a crystal structure of the protein in complex with a dipeptide, crystallisation conditions suitable for crystallography-based fragment screening, an inhibition assay and fragment hits in the active site and an allosteric site. These molecules provide a promising starting point for the development of more specific and potent PgDPP11 inhibitors.

## SCIENTIFIC BACKGROUND

Periodontitis is the most common chronic inflammatory disease of humans worldwide, affecting nearly half of adults in the United Kingdom and the United States of America (1). *P. gingivalis* is a gram-negative black-pigmented anaerobe and a major pathogen associated to chronic Periodontitis (2). Recently, considerable attention has been drawn to this organism due to reports associating Periodontitis to systemic diseases. *P. gingivalis* translocates to several organs as result of bacteremia, which occurs during activities such as brushing, flossing, chewing and dental practices (3) followed by, as recently proposed in some cases, macrophage hijacking (4). A recent study from The Forsyth Institute and Harvard School of Dental Medicine showed *P. gingivalis* arterial colonisation in 100% of patients with cardiovascular disease (5). Dominy et al., 2019 (6) showed that *P.gingivalis* was present in the brain of AD patients and levels of the toxic protease gingipains correlated with tau and ubiquitin pathology. The authors developed a small molecule gingipain inhibitor called COR388 currently in phase 2/3 clinical study, which was capable of reducing the bacterial load of an established *P.gingivalis* brain infection <https://gaintrial.com/en/>. Our collaborators, Prof. Takayuki and Ohara Nemoto, have recently demonstrated that recombinant DPP4 from *P. gingivalis* degrades human GLP-1 and GIP *in vitro*. Moreover, intravenous injection of PgDPP4 in mice decreased plasma GLP-1, shedding light on the well-established correlation between Periodontitis and type 2 diabetes (7). Other systemic conditions related to *P. gingivalis* include rheumatoid arthritis (8), oral and pancreatic cancers (9) (10), as well as respiratory diseases (11).

*P. gingivalis* is an assacharolyte and therefore does not ferment carbohydrates; instead, it uses proteinaceous substrates as carbon and energy sources (12). The bacterium employs several proteases to break down protein and peptides into amino acids and degrade them further via specific pathways.

PgDPP11 is a homodimeric 160 kDa serine protease (catalytic triad His85, Asp227 and Ser655) recently discovered in *P. endodontalis* and later identified in *P. gingivalis* by homology search (13). Due to its specificity for Asp/Glu in the P1 position, DPP11 discovery correlates with the observation that aspartate and glutamate are the most intensively consumed amino acids in *P. gingivalis* (14). Indeed, the only *P. gingivalis* periplasmic protease whose knockout shows growth impairment is *dpp11*-knockout (13). In this way, DPP11 is critical for the bacterium energy metabolism and its absence in mammals positions the enzyme further as an attractive drug target.

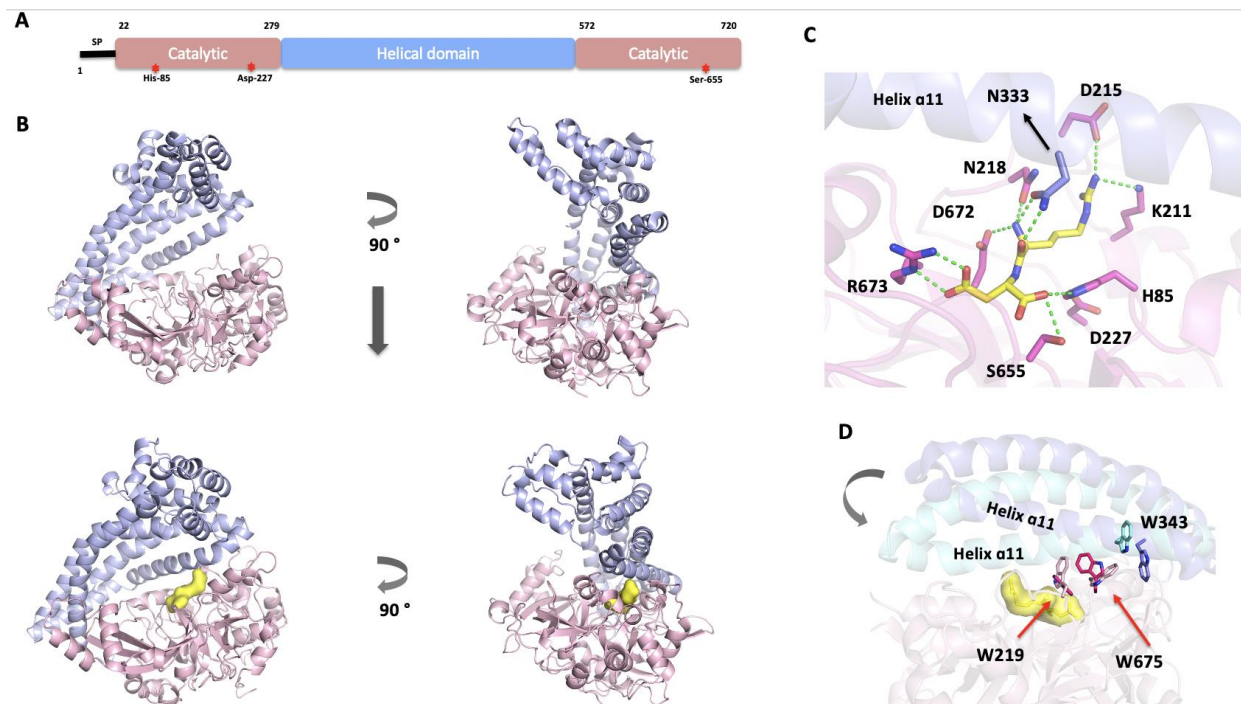
## RESULTS – THE TEP

## Protein purified

In order to express soluble PgDPP11 in *E. coli*, we designed a construct lacking the N-terminal signal peptide (amino acids 1-21), which addresses the protein to the inner membrane where it faces the bacterial periplasmic space. The final protein expressed encompasses amino acids 22-720 (**Fig 1A**). For isothermal titration experiments we expressed and purified the inactive mutant S655A.

## Structures

We have grown monoclinic (space group *C2*) crystals of PgDPP11<sub>22-720</sub> in complex with the peptide RD (**Fig 1B**), with 2 molecules in the asymmetric unit, which yielded diffraction data up to 1.8 Å. The protein occurs as a dimer with an overall fold similar to that of the unbound enzyme. Its bilobal architecture comprises an upper entirely helical domain and a lower domain containing the catalytic triad, which are separated by a cleft. The catalytic domain (Asp22 – Thr279 and Asp572 – Pro720) is composed of a core motif of two beta-barrels, whose members share a chymotrypsin-like fold and similar catalytic mechanisms. The helical domain (residues His280 – Pro571) is responsible for the specificity of the enzyme and is posed capping the catalytic fold. Remarkably, the enzyme undergoes a large conformational change upon peptide binding, resulting in a fully formed active site. The bound peptide is anchored by polar interactions between the main chain of its P2 residue (arginine in this case) and the side chains of Asn333, Asn218 and Asp672 (**Fig 1C**). A rotation movement brings the helical domain 22° closer to the catalytic domain. While inspecting conformational changes at amino acids side chain level, we noticed that Trp343 (located in the helix  $\alpha$ 11) and Trp675 (adjacent to the active site) display the most striking difference, the latter is in a perpendicular orientation related to the former, which has rotated 180° (**Fig 1D**). We denominate this configuration as “locked”, with atoms CZ3 and CH2 at an average distance of 4 Å from Trp343 side chain atoms. After the peptide binding event, this distance is increased to more than 8 Å, and these residues are now in an “unlocked” configuration (**Fig 1D**) to prevent clashes between them. We hypothesise that such distinct re-arrangement is part of the enzyme closure mechanism and could therefore be targeted for inhibitor development.

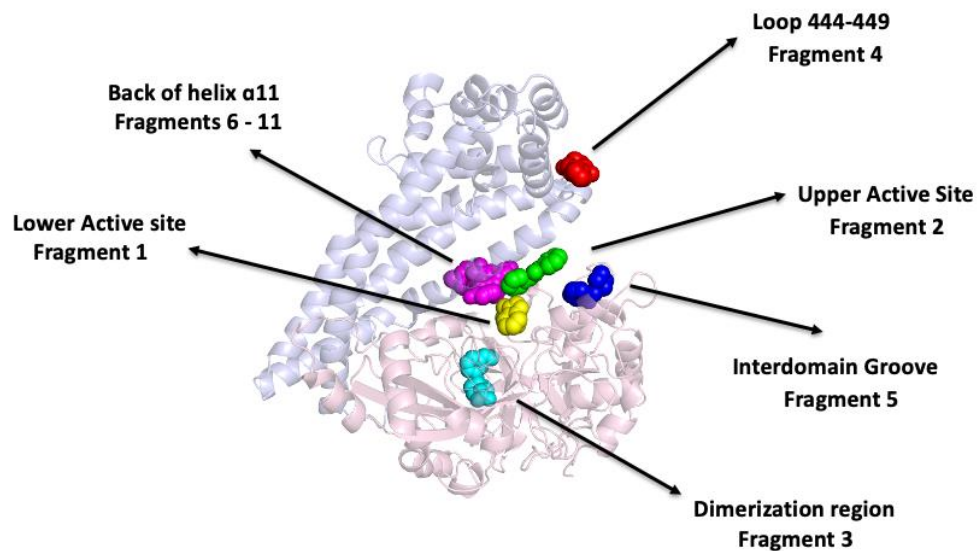


**Figure 1** Overall structure of PgDPP11. **(A)** PgDPP11 domain organization. The domains are represented as boxes and their borders are indicated. SP is signal peptide. Catalytic domain is in pink and helical domain is in blue. The catalytic triad is shown as “red stars”. **(B)** Cartoon representation of PgDPP11<sub>20-720</sub> structure. Upper panel shows overall structure of unbound PgDPP11<sub>22-720</sub>. Lower panel shows the overall structure of PgDPP11<sub>22-720</sub> in complex with dipeptide Arg-Asp (shown as yellow surface). **(C)** Close-up view of PgDPP11 active site. The peptide is shown in yellow and polar interactions are depicted as dashed green lines. Domains are colored as in **(A)**.

## Chemical matter

We have performed X-ray crystallography fragment screening at the XChem facility to identify ligands with potential to be developed into PgDPP11 inhibitors. We observed 11 fragments distributed in 6 binding pockets. Fragment **1** is located in the active site close to the catalytic triad (lower active site); Fragment **2**

interacts with the N-anchor Asn333 in helix  $\alpha$ 11, which constitutes the active site portion located in the helical domain (upper active site); Fragment **3** is found in the dimerization region, interacting with residues located in strands  $\beta$ 14 and  $\beta$ 15, forming the  $\beta$ -hairpin structure. Fragment **4** is located between loop Ala444 – Ser449 and helix  $\alpha$ 11 (Pro318-Thr347); Fragment **5** binds in a groove formed by elements helix  $\alpha$ 9 and helix  $\alpha$ 26 adjacent to active site (12 Å from fragment **1**). Fragments **6-11** are accommodated between Trp675 and Trp343, on the back of helix  $\alpha$ 11 (**Fig 2**), we hypothesise that these residues are involved in the mechanism of the protein conformational change upon peptide binding and therefore are good candidates to be developed further into highly selective inhibitors.

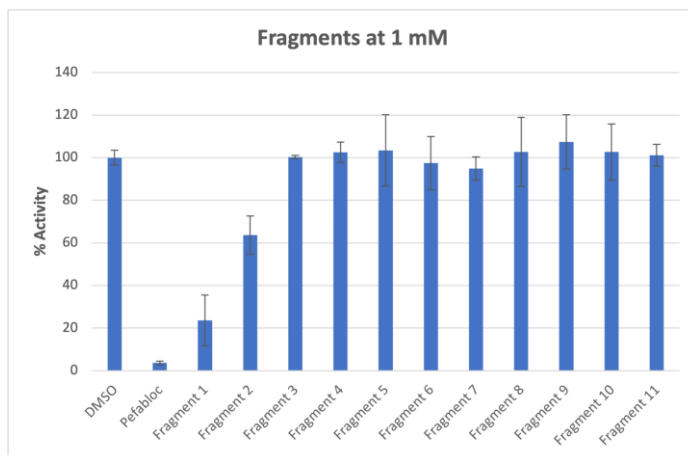


**Figure 2** Crystallography-based fragment screening of PgDPP11. The fragment hits are observed in distinct regions of the enzyme.

## Assays

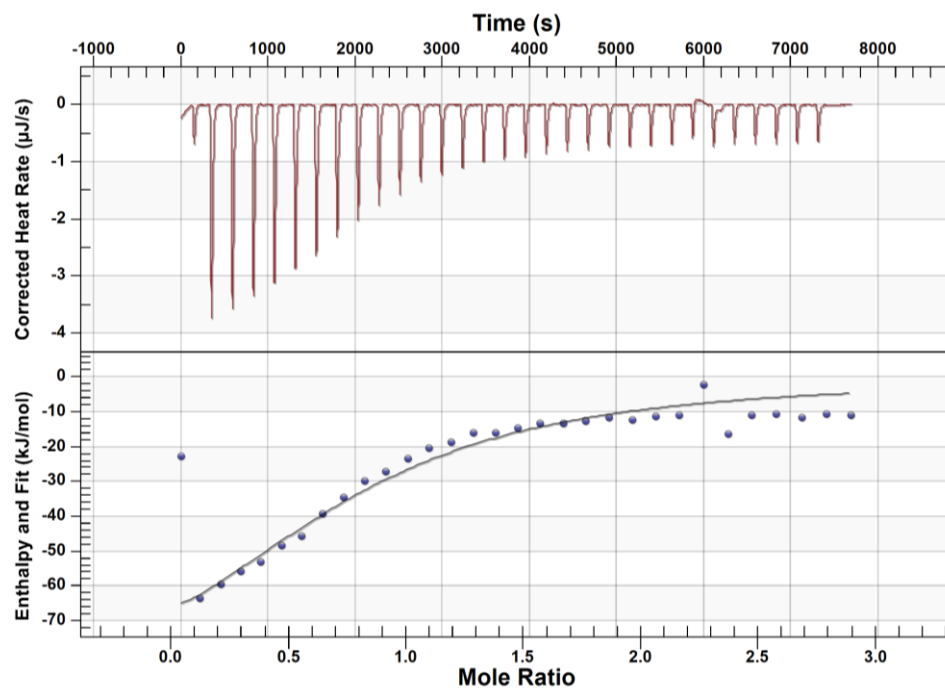
To characterise the binding of fragment hits we employed a fluorescence-based assay where we monitor the hydrolysing activity of PgDPP11 against the substrate Leu-Asp-MCA (4-methylcoumaryl-7-amide). We followed fluorescence intensity with excitation at 380nm and emission at 460nm.

Remarkably, we observed a clear effect on activity even though fragments are known to be weak binders. Fragments **1** and **2** showed inhibitory properties at 1 mM (**Fig 3**). Fragment **1** displayed around 80% inhibition while Fragment **2** displayed around 40% inhibition.



**Figure 3** Inhibition profile of PgDPP11 XChem fragment hits. Peflaboc was used as a positive control, .

To further verify the binding of candidate inhibitor molecules we established experimental conditions to perform Isothermal Titration Calorimetry measurements by titrating the tetrapeptide Arg-Asp-Val-Trp into the inactive DPP11 (S655A), in the presence of 5% DMSO (**Fig 4**).



**Figure 4** Isothermal Titration Calorimetry of inactive PgDPP11 S655A and the tetrapeptide Arg-Asp-Val-Trp. Time-dependent deflection of heat for each injection. Integrated calorimetric data for the respective interactions, the continuous line represents the best fit using a one-site binding model.

**IMPORTANT:** Please note that the existence of small molecules within this TEP indicates only that chemical matter might bind to the protein in potentially functionally relevant locations. The small molecule ligands are intended to be used as the basis for future chemistry optimisation to increase potency and selectivity and yield a chemical probe or lead series. As such, the molecules within this TEP should not be used as tools for functional studies of the protein, unless otherwise stated, as they are not sufficiently potent or well-characterised to be used in cellular studies.



## CONCLUSION

We have solved the first crystal structure of PgDPP11 in complex with a peptide to elucidate the enzyme's specificity and binding mechanism to assist the development of inhibitors. Next, we have performed a crystallography-based fragment screening campaign and identified molecules bound to different regions of PgDPP11 with potential for further inhibitor development. Notably, two fragments found at the active site significantly inhibited the enzyme. Fragment **1** located close to the conserved catalytic residues, and Fragment **2** binding to residues originated from the less conserved helical domain. Additionally, fragments located at an allosteric site (back of helix 11, close to Trp675 and Trp343) might provide a unique opportunity for the development of highly selective inhibitors. We envisage that PgDPP11 inhibitors might represent a new class of antibiotics targeting *P. gingivalis* not only for the treatment of Periodontitis, but also for systemic diseases such Alzheimer's and type 2 diabetes.

## TEP IMPACT

The fragments identified in the active site of PgDPP11 and also at the allosteric binding site close to Trp675 and Trp343 are currently being progressed in our group employing deep machine-learning approaches for linking and merging fragments. More potent and selective compounds will be tested in bacterial growth assays in the lab of Prof. Takayuki Nemoto at the University of Nagasaki. We are currently writing grant proposals to secure resources for a more extensive medicinal chemistry campaign. In our study proposals, the optimised fragments discovered here will play an important role in helping to elucidate *P. gingivalis* impact in several systemic diseases.

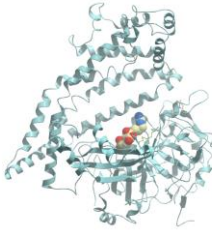
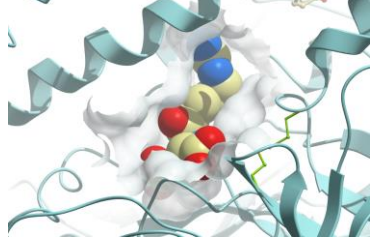
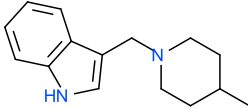
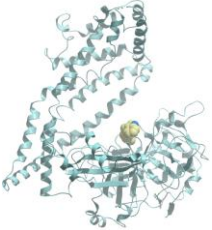
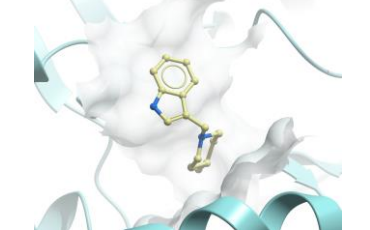
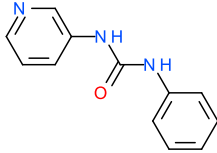
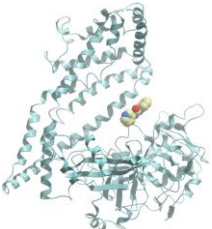

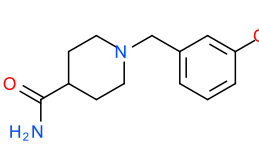
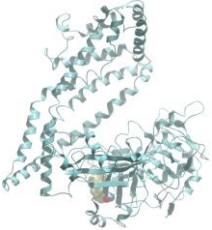
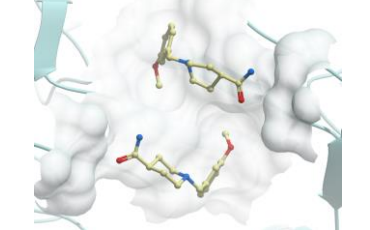
## FUNDING INFORMATION

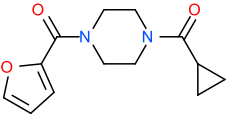
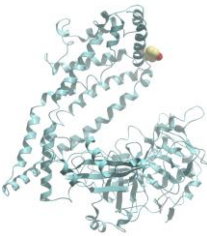
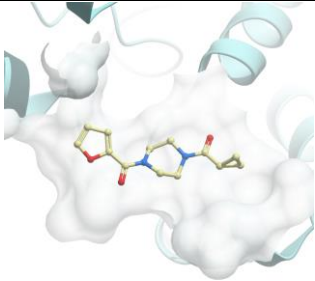
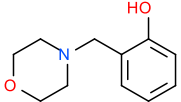
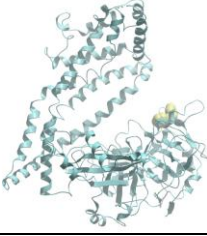
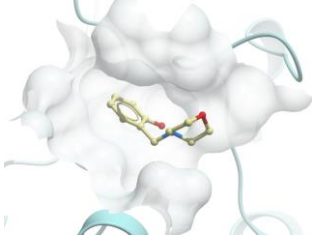
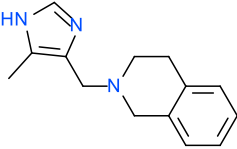
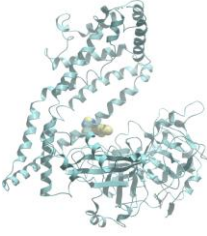
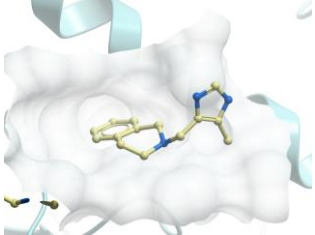
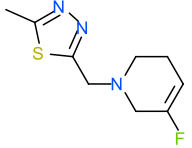
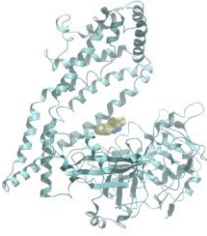
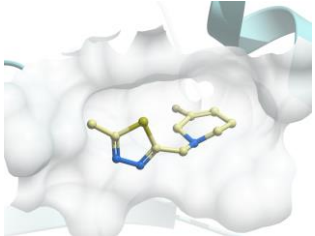
The work performed at the CMD has been funded by a grant from the Wellcome [106169/ZZ14/Z].

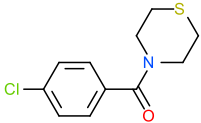
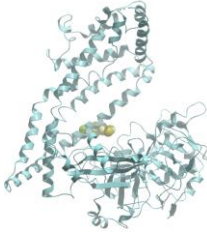
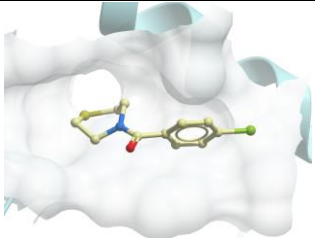
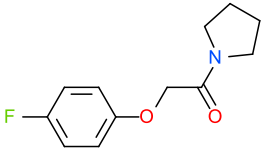
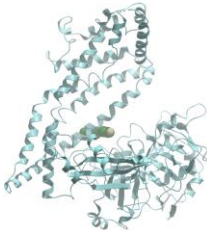
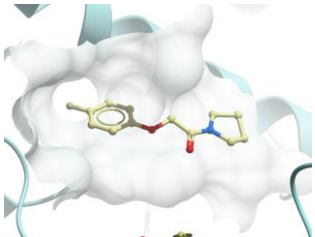
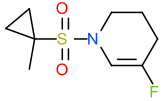
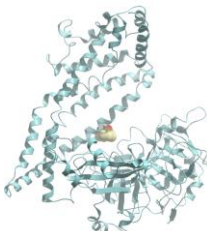
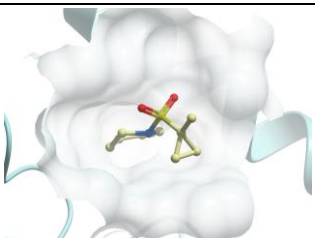
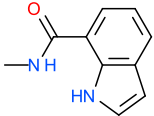
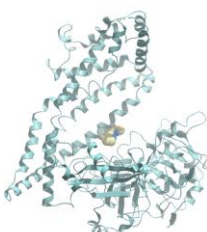
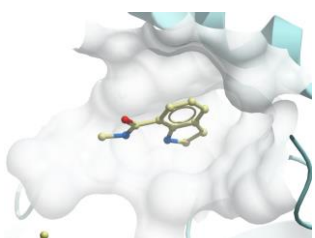
## ADDITIONAL INFORMATION

### Structure Files

For more information regarding any aspect of TEPs and the TEP programme, please contact [teps@cmd.ox.ac.uk](mailto:teps@cmd.ox.ac.uk)

PDB ID	Resolution (Å)	Ligand Details	Binding site	Binding pocket
<a href="#">7R51</a>	1.8	Dipeptide Arg-Asp		
<a href="#">5SDC</a>	1.93	Fragment 1 ( <b>Z2856434912</b> ):  3-((4-methylpiperidin-1-yl)methyl)-1H-indole		
<a href="#">5SDI</a>	1.90	Fragment 2 ( <b>Z44592329</b> ):  1-phenyl-3-(pyridin-3-yl)urea		
<a href="#">5SDH</a>	2.31	Fragment 3 ( <b>Z2856434854</b> ):  1-(3-methoxybenzyl)piperidine-4-carboxamide		

<a href="#">5SDJ</a>	2.04	<p><b>Fragment 4 (Z32327641):</b></p>  <p>(4-(cyclopropanecarbonyl)piperazin-1-yl)(furan-2-yl)methanone</p>		
<a href="#">5SDQ</a>	1.92	<p><b>Fragment 5 (Z2856434887):</b></p>  <p>2-(morpholinomethyl)phenol</p>		
<a href="#">5SDD</a>	1.84	<p><b>Fragment 6 (Z2856434879):</b></p>  <p>3-((5-methyl-1H-imidazol-4-yl)methyl)-1H-indole</p>		
<a href="#">5SDE</a>	1.85	<p><b>Fragment 7 (Z1619978933):</b></p>  <p>2-((5-fluoro-3,6-dihydropyridin-1(2H)-yl)methyl)-5-methyl-1,3,4-thiadiazole</p>		

<a href="#">5SDN</a>	2.02	<p><b>Fragment 8 (Z437584380):</b></p>  <p>(4-chlorophenyl)(thiomorpholino)methanone</p>		
<a href="#">5SDO</a>	2.05	<p><b>Fragment 9 (Z19735067):</b></p>  <p>2-(4-fluorophenoxy)-1-(pyrrolidin-1-yl)ethan-1-one</p>		
<a href="#">5SDP</a>	2.19	<p><b>Fragment 10 (Z2277255954):</b></p>  <p>5-fluoro-1-((1-methylcyclopropyl)sulfonyl)-1,2,3,6-tetrahydropyridine</p>		
<a href="#">5SDR</a>	2.08	<p><b>Fragment 11 (Z1273312153):</b></p>  <p>N-methyl-1H-indole-7-carboxamide</p>		

## Materials and Methods

### Protein expression and purification

Vector:pNIC-CH

Entry clone accession: B2RID1

Cell line: *E. coli* BL21(DE3)pLysS

Tag and additions: the protein has a C-terminal 6x His-tag

MDEGMWLMQQLGRKYAQMKERGLKMKEYDLYNPNGTSLKDAVVLFDGGCTGEVVS DRGLVLTNHHCGYD MIQAHSTL  
EHNYLENGFWAMREADELPNKDISVVFIDKIEDVTDYVKKELKAIKDPNSMDYLSPKYLQKLADKKAGKNFSAKNPGLSVEIK  
AFYGGNLYLMFTKKTYYTDVRLVGAPPSSIGKFGADTDNWIWPRHTGDFSIFRIYADKNGNPAPYSEDNVPLKPKRFFNISLGG  
VQENDYAMIMGFP GTT HRYFTASEVDEWKSIDNDIRMRDIRQGVMLREMLADPQIKIMYSAKYAASQNA YKRAIGANW  
AIKTRGLRQNKQAMQDRLIAWGA KQGTPRYEEAVHEIDATVAKRADLRRRYWMI EEGIIRGIEFARSP IETEDETKALQGND  
ASARKEAIDKIRTRYSKFANKDYSAEVDK KAVAVAMLTEYLKEIPYENLPLHLRLVKDRFAGDVQAYVDDIFARSVFGSEAQFDA  
FAAVPSVEKLAEDPMVLFASSVFDEYRKL YNELRPYDDPILRAQR TYIAGLLEMDGDQDQFPDANLTLRFTY GQVKGYSPRD  
NVVYGHQTTLDGVM EKEDPDNWEFVVDPKL KAVYERKDFGRYADRSGRMPVAF CATTHTTGGNSGSPVMNANGELIGL  
NFDRNWEVGGDIQYLADYQRSIIVDIRYVLLVIDKVG GCQRLLEMNIVPAHHHHHH

### Inactive mutant S655A

Vector:pNIC-CH

Entry clone accession: B2RID1

Cell line: *E. coli* BL21(DE3)pLysS

Tag and additions: the protein has a C-terminal 6x His-tag

MDEGMWLMQQLGRKYAQMKERGLKMKEYDLYNPNGTSLKDAVVLFDGGCTGEVVS DRGLVLTNHHCGYD MIQAHSTL  
EHNYLENGFWAMREADELPNKDISVVFIDKIEDVTDYVKKELKAIKDPNSMDYLSPKYLQKLADKKAGKNFSAKNPGLSVEIK  
AFYGGNLYLMFTKKTYYTDVRLVGAPPSSIGKFGADTDNWIWPRHTGDFSIFRIYADKNGNPAPYSEDNVPLKPKRFFNISLGG  
VQENDYAMIMGFP GTT HRYFTASEVDEWKSIDNDIRMRDIRQGVMLREMLADPQIKIMYSAKYAASQNA YKRAIGANW  
AIKTRGLRQNKQAMQDRLIAWGA KQGTPRYEEAVHEIDATVAKRADLRRRYWMI EEGIIRGIEFARSP IETEDETKALQGND  
ASARKEAIDKIRTRYSKFANKDYSAEVDK KAVAVAMLTEYLKEIPYENLPLHLRLVKDRFAGDVQAYVDDIFARSVFGSEAQFDA  
FAAVPSVEKLAEDPMVLFASSVFDEYRKL YNELRPYDDPILRAQR TYIAGLLEMDGDQDQFPDANLTLRFTY GQVKGYSPRD  
NVVYGHQTTLDGVM EKEDPDNWEFVVDPKL KAVYERKDFGRYADRSGRMPVAF CATTHTTGGNAGSPVMNANGELIGL  
NFDRNWEVGGDIQYLADYQRSIIVDIRYVLLVIDKVG GCQRLLEMNIVPAHHHHHH

PgDPP11 containing plasmid was transformed in BL21(DE3)pLysS. The cells were grown in LB-medium containing 100 µg/mL ampicillin and 34 µg/mL chloramphenicol. After 3 h at 37°C, protein expression was induced by the addition of 0.5 mM isopropyl-1-thio-D-galactopyranoside (IPTG). Cells were then allowed to grow for 4 h and were harvested by centrifugation at 4,000g for 10 minutes. For protein purification, cells were resuspended in 10 mM Hepes-NaOH pH 8.0, 150 mM NaCl. Cell debris was removed by centrifugation at 25,000g for 45 minutes at 4°C and the supernatant was subjected to affinity chromatography on 5ml HisTrap™ (GE Healthcare) previously equilibrated with lysis buffer. Bound protein was eluted in lysis buffer containing 500 mM imidazole. Further purification was performed by size exclusion chromatography (SEC) on a HiLoad 26/60 Superdex 200 (GE Healthcare) column previously equilibrated with 10 mM Hepes-NaOH pH 7.4, 100 mM NaCl. Purified protein was concentrated using 20 mL concentrators with an appropriate molecular weight cut-off (Vivaspin® 50,000 MWCO, Sartorius).

### Crystallisation

Crystals were grown by vapour diffusion method. PgDPP11 was crystallised at 28mg/mL and incubated with 10x fold excess of peptide Arg-Leu at 20°C, using the screen JCSG in the condition: 20% PEG3350 - 0.2M sodium

malonate. The crystallisation trials were performed using the nanodrop-dispensing Mosquito robot. The crystal was cryo-protected in a solution consisting of reservoir solution supplemented with 25% Ethylene Glycol and then flash-cooled in liquid nitrogen.

### Structure determination

Diffraction data were collected at the Diamond Light Source beamline I04, and processed using the CCP4 program suite (15). PgDPP11 was crystallised in the monoclinic space group *C2* with two molecules in the asymmetric unit. The structure was solved by molecular replacement using the program *PHASER*(16) and the *unbound PgDPP11* structure (PDB code 5JWF) as search model. The structure was refined using *PHENIX* (17), followed by iterative cycles of model building in *COOT* (18).

### Crystallography-based fragment screening

For the fragment screening campaign, PgDPP11 was crystallised in Morpheus screen, condition A3: 0.06 M Divalents - 0.1M Buffer system 1 pH 6.5 - 50% v/v Precipitant Mix3.

For soaking, 50 nL of each fragment compound from the XChem fragment library (final concentration of 50 mM) was added to a crystallisation drop using an ECHO acoustic liquid handler dispenser at the Diamond Light Source XChem facility. Crystals were soaked for two hours with fragments from the Diamond-SGC Poised Library before being harvested using XChem SHIFTER technology, cryo-cooled in liquid nitrogen and data sets collected at the beamline I04-1 in “automated unattended” mode. The XChem Explorer pipeline (28) was used for structure solution with parallel molecular replacement using *DIMPLE* (29), followed by map averaging and statistical modelling to identify weak electron densities generated from low occupancy fragments using *PANDDA* software (30). Coordinates and structure factors for exemplary data sets with bound fragments were deposited in the RCSB Protein Data Bank.

### Inhibition assays

PgDPP11 activity was measured by peptidase assay using Leu-Asp-MCA. Firstly, 0.62nM protein (0.05ng/μl) was mixed with 100 or 200uL reaction buffer composed of 50mM sodium phosphate (pH7), 100mM NaCl, and 5mM EDTA. Then, 20uM MCA-peptide was added into reaction mixture and incubated for 1h at 37°C. Finally, the sample was transferred to a 96-well flat bottom black microplate (Greiner), and the hydrolysing activity of PgDPP11 toward Leu-Asp-MCA was monitored by fluorescence intensity with excitation at 380nm and emission at 460nm on a PHERAstar FS microplate reader (BMG LABTECH). The inhibitory effects of XChem fragments were measured at 1mM in 100% DMSO. Pefabloc, a specific, potent and irreversible inhibitor of serine proteases was used as a positive control at 2 mM.

### Isothermal Titration Calorimetry

The experiment was carried out in 10 mM Hepes-NaOH pH 7.4, 100 mM NaCl, 5% DMSO. Both the enzymes and the peptides were dissolved in the same buffer. The bindings were analysed with a Nano ITC (TA instruments) equilibrated at 20°C. One aliquot of 4 μl and 30 aliquots of 8.0 μl of the peptide solution were injected at a rate of 0.5 μl/s into 200 μl of the protein solution under constant stirring at 350 rpm at the specified concentrations. 200 μM of the tetrapeptide RDLW was titrated into 20 μM of PgDPP11 inactive mutant S655A.

## References

1. Eke, P. I., Dye, B. A., Wei, L., Slade, G. D., Thornton-Evans, G. O., Borgnakke, W. S., Taylor, G.



- W., Page, R. C., Beck, J. D., and Genco, R. J. (2015) Update on Prevalence of Periodontitis in Adults in the United States: NHANES 2009 to 2012. *J. Periodontol.* **86**, 611–622
2. Sakanaka, A., Takeuchi, H., Kuboniwa, M., and Amano, A. (2016) Dual lifestyle of *Porphyromonas gingivalis* in biofilm and gingival cells. *Microb. Pathog.* **94**, 42–47
  3. Forner, L., Larsen, T., Kilian, M., and Holmstrup, P. (2006) Incidence of bacteremia after chewing, tooth brushing and scaling in individuals with periodontal inflammation. *J. Clin. Periodontol.* **33**, 401–407
  4. Hajishengallis, G. (2015) Periodontitis: From microbial immune subversion to systemic inflammation. *Nat. Rev. Immunol.* **15**, 30–44
  5. Mougeot, J. L. C., Stevens, C. B., Paster, B. J., Brennan, M. T., Lockhart, P. B., and Mougeot, F. K. B. (2017) *Porphyromonas gingivalis* is the most abundant species detected in coronary and femoral arteries. *J. Oral Microbiol.* **9**, 1–9
  6. Dominy, S. S., Lynch, C., Ermini, F., Benedyk, M., Marczyk, A., Konradi, A., Nguyen, M., Haditsch, U., Raha, D., Griffin, C., Holsinger, L. J., Arastu-Kapur, S., Kaba, S., Lee, A., Ryder, M. I., Potempa, B., Mydel, P., Hellvard, A., Adamowicz, K., Hasturk, H., Walker, G. D., Reynolds, E. C., Faull, R. L. M., Curtis, M. A., Dragunow, M., and Potempa, J. (2019) *Porphyromonas gingivalis* in Alzheimer’s disease brains: Evidence for disease causation and treatment with small-molecule inhibitors. *Sci. Adv.* **5**, 1–21
  7. Ohara-Nemoto, Yuko, nemoto, takayuki K. (2017) Degradation of Incretins and Modulation of Blood Glucose Levels by Periodontopathic Bacterial Dipeptidyl
  8. Chou, Y. Y., Lai, K. L., Chen, D. Y., Lin, C. H., and Chen, H. H. (2015) Rheumatoid arthritis risk associated with periodontitis exposure: A nationwide, population-based cohort study. *PLoS One.* **10**, 1–10
  9. Michaud, D. S., Izard, J., Wilhelm-Benartzi, C. S., You, D. H., Grote, V. A., Tjønneland, A., Dahm, C. C., Overvad, K., Jenab, M., Fedirko, V., Boutron-Ruault, M. C., Clavel-Chapelon, F., Racine, A., Kaaks, R., Boeing, H., Foerster, J., Trichopoulou, A., Lagiou, P., Trichopoulos, D., Sacerdote, C., Sieri, S., Palli, D., Tumino, R., Panico, S., Siersema, P. D., Peeters, P. H. M., Lund, E., Barricarte, A., Huerta, J. M., Molina-Montes, E., Dorransoro, M., Ramón Quirós, J., Duell, E. J., Ye, W., Sund, M., Lindkvist, B., Johansen, D., Khaw, K. T., Wareham, N., Travis, R. C., Vineis, P., Bas Bueno-De-Mesquita, H., and Riboli, E. (2013) Plasma antibodies to oral bacteria and risk of pancreatic cancer in a large European prospective cohort study. *Gut.* **62**, 1764–1770
  10. Javed, F., and Warnakulasuriya, S. (2016) Is there a relationship between periodontal disease and oral cancer? A systematic review of currently available evidence. *Crit. Rev. Oncol. Hematol.* **97**, 197–205
  11. Paju, S., and Scannapieco, F. A. (2007) Oral biofilms, periodontitis, and pulmonary infections. *Oral Dis.* **13**, 508–512
  12. Rouf, S. M. A., Ohara-Nemoto, Y., Ono, T., Shimoyama, Y., Kimura, S., and Nemoto, T. K. (2013) Phenylalanine 664 of dipeptidyl peptidase (DPP) 7 and Phenylalanine 671 of DPP11 mediate preference for P2-position hydrophobic residues of a substrate. *FEBS Open Bio.* **3**, 177–183
  13. Ohara-Nemoto, Y., Shimoyama, Y., Kimura, S., Kon, A., Haraga, H., Ono, T., and Nemoto, T. K. (2011) Asp- and Glu-specific novel dipeptidyl peptidase 11 of *porphyromonas gingivalis* ensures utilization of Proteinaceous energy sources. *J. Biol. Chem.* **286**, 38115–38127
  14. Takahashi, N., Sato, T., and Yamada, T. (2000) Metabolic pathways for cytotoxic end product formation from glutamate- and aspartate-containing peptides by *Porphyromonas gingivalis*. *J. Bacteriol.* **182**, 4704–4710
  15. Winn, M. D., Ballard, C. C., Cowtan, K. D., Dodson, E. J., Emsley, P., Evans, P. R., Keegan, R. M.,

- Krissinel, E. B., Leslie, A. G. W., McCoy, A., McNicholas, S. J., Murshudov, G. N., Pannu, N. S., Potterton, E. A., Powell, H. R., Read, R. J., Vagin, A., and Wilson, K. S. (2011) Overview of the CCP4 suite and current developments. *Acta Crystallogr. Sect. D Biol. Crystallogr.* **67**, 235–242
16. McCoy, A. J., Grosse-Kunstleve, R. W., Adams, P. D., Winn, M. D., Storoni, L. C., and Read, R. J. (2007) Phaser crystallographic software. *J. Appl. Crystallogr.* **40**, 658–674
  17. 2011, A. et al (2013) The Phenix Software for Automated Determination of Macromolecular Structures. **55**, 94–106
  18. Emsley, P., and Cowtan, K. (2004) Coot: Model-building tools for molecular graphics. *Acta Crystallogr. Sect. D Biol. Crystallogr.* **60**, 2126–2132

**We respectfully request that this document is cited using the DOI value as given above if the content is used in your work.**